Adsorption site and orientation of pyridine on Cu{110} determined by photoelectron diffraction

Cite as: J. Chem. Phys. **110**, 9666 (1999); https://doi.org/10.1063/1.478930
Submitted: 09 October 1998 . Accepted: 22 February 1999 . Published Online: 05 May 1999

T. Gießel, O. Schaff, R. Lindsay, P. Baumgärtel, M. Polcik, A. M. Bradshaw, A. Koebbel, T. McCabe, M. Bridge, D. R. Lloyd, and D. P. Woodruff

Adsorption site and orientation of pyridine on Cu{110} determined by photoelectron diffraction

T. Gießel, O. Schaff, R. Lindsay, P. Baumgärtel, M. Polcik, and A. M. Bradshaw
Fritz-Haber-Institut der Max-Planck-Gesellschaft, Faradayweg 4–6, 14195 Berlin, Germany

A. Koebbel, T. McCabe, M. Bridge, and D. R. Lloyd
Department of Chemistry, Trinity College, Dublin, Ireland

D. P. Woodruff
Department of Physics, University of Warwick, Coventry CV4 7AL, United Kingdom

(Received 9 October 1998; accepted 22 February 1999)

The local adsorption geometry of pyridine on Cu{110} has been determined quantitatively using photoelectron diffraction in the scanned-energy mode. At high coverages the molecule adsorbs nearly atop a Cu atom in the close-packed rows with a N–Cu bond length of 2.00 Å. Moreover, the Cu–N axis and the molecular (C_2) axis are inclined by 8° and 20°, respectively, to the surface normal. The result shows that not only the adsorption site of the emitter (in this case the N atom) but also the position of relatively light scatterers (the C atoms) can be determined by photoelectron diffraction. © *1999 American Institute of Physics.* [S0021-9606(99)70119-4]

I. INTRODUCTION

Benzene (C_6H_6) and pyridine (C_5H_5N) adsorbed on low index single crystal metal surfaces represent model systems for the study of the interaction of aromatic compounds with metals.[1–5] Whereas the benzene–metal bond is dominated by the interaction with the π-system, pyridine has the additional option of bonding to the metal via the lone pair electrons of the nitrogen. Although the data base is still relatively small, pyridine is thought to adopt—depending on which type of electronic interaction dominates the bonding—a geometry in which the molecular plane is perpendicular or parallel to the surface, as depicted in Figs. 1(a) and 1(b). The tilted geometry shown in Fig. 1(c) is expected if both bonding modes are important. Pyridine adsorption has been investigated on silver,[6,7] nickel,[8–11] ruthenium,[12,13] palladium,[14] copper,[12,15,16] iridium,[17] platinum[12,16,18,19] and rhodium[20] surfaces. Often the molecule adopts for steric reasons an ''upright'' (perpendicular or near-perpendicular) geometry at high coverages. The formation of an α-pyridyl species (C_5H_4N) at room temperature or above has also been reported for some systems;[8,12,13,16–20] possible bonding geometries are shown in Figs. 1(d) and 1(e).

Almost all the determinations of the local geometry of adsorbed pyridine have been based on qualitative, or at best, semiquantitative data from vibrational spectroscopy, angle-resolved photoemission or near-edge x-ray absorption fine structure (NEXAFS). To our knowledge, only one quantitative structure determination has been carried out so far; our earlier study on Ni{111} (Ref. 11) using photoelectron diffraction in the scanned energy mode (PhD) showed that the molecule bonds via the N atom almost atop a Ni atom with an angle of of 18° (+2/−4)° between the N–Ni bond and the surface normal. The bond length was found to be 1.97 (±0.03) Å. Unfortunately, it was not possible to locate the positions of the C atoms and thus to determine the inclination of the ring plane, although a previous NEXAFS study[10] had indicated that this is also tilted by about 20° to the surface normal, i.e., indicating that the Ni–N bond and the aromatic ring are coplanar.

In the present paper we describe a N 1*s* photoelectron diffraction study of the local adsorption geometry of pyridine on Cu(110), a system in which the molecular plane is thought to remain perpendicular, or essentially perpendicular, to the surface over the whole coverage range. For obvious reasons we have concentrated on determining not only the adsorption site and the Cu–N bond length, but also the orientation of the aromatic ring with respect to the surface. Despite the relatively weak scattering cross section of carbon compared to that of the substrate atoms, we show that it is also possible to obtain this kind of information, albeit at lower precision, from the N 1*s* diffraction data.

Pyridine adsorption on silver and copper surfaces is particularly significant for understanding the surface-enhanced Raman effect. Using attenuated total reflection a first layer enhancement of a factor of 40 has recently been measured for pyridine on a Cu{110} electrode surface.[21]

II. STRUCTURE DETERMINATION WITH PhD

Photoelectron diffraction in the scanned energy mode involves the measurement of the intensity of an adsorbate core-level photoelectron line at a pre-selected emission angle as a function of photon energy, and thus of photoelectron energy.[22] Synchrotron radiation is required for the experiment, since conventional soft x-ray sources for photoelectron spectroscopy have lines at only a few fixed photon energies. The dependence of photoelectron intensity on kinetic energy is modulated by the interference between the directly emitted component of the photoelectron wave and the components that arise from elastic scattering at neighboring atoms. The modulations depend in turn on the contributing path length

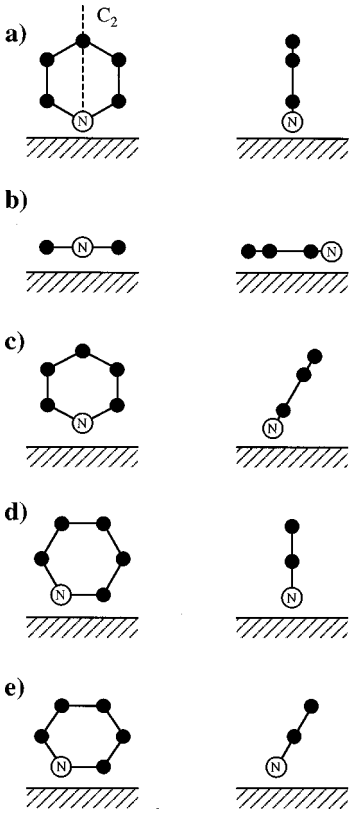

FIG. 1. Different adsorption geometries of pyridine on metal surfaces.

differences and thus provide information on the local geometry of the emitter atom. The latter is extracted in a similar way to the method used in quantitative low energy electron diffraction (LEED) studies by comparing experimental modulation functions with simulated curves calculated using multiple scattering theory. The modulation function is defined by

$$\chi_{\mathrm{ex}}(\theta,\phi,k)=(I(k)-I_0(k))/I_0(k), \tag{1}$$

where I and I_0 are the diffractive and nondiffractive intensities, θ and ϕ are the polar and azimuthal emission angles, and k is the modulus of the photoelectron wave vector. $I_0(k)$ is obtained by performing a smooth fit to $I(k)$ with a spline function (assuming that the nondiffractive part of the intensity changes only slowly as a function of energy).

In our integrated approach[23] to photoelectron diffraction quantitative structure determination generally proceeds in two stages. A direct method is used to determine the adsorption site employing the full set of data and calculating the so-called projection integrals.[24] The underlying physical principle is that modulation functions measured in directions which correspond to 180° scattering from a near-neighbor substrate atom (''the backscattering geometry'') are typically dominated by this event and show particularly strong intensity modulations. This component of the modulation function can thus be described quite well within the single scattering approximation with only one scatterer taken into account. The method produces a three-dimensional intensity map of the space around the emitter, with maximum values of the projection integral in regions corresponding to the nearest neighbor backscatters. The second stage is a full quantitative structural analysis using an iterative ''trial-and-error'' procedure which involves a comparison of a reduced set of usually 6–10 experimental spectra with the results of multiple scattering simulations based on trial model structures. These calculations have been performed on the basis of an expansion of the final state wave function into a sum over all scattering pathways which the electron can take from the emitter atom to the detector outside the sample. A magnetic quantum number expansion of the free electron propagator has been used to calculate the scattering contribution of an individual scattering path.[25] Double and higher order scattering events were treated by means of the reduced angular momentum expansion (RAME).[26] The finite energy resolution and angular acceptance of the electron analyzer are included. Anisotropic vibrations for the emitter atom and isotropic vibrations for the scattering atoms are also taken into account. The comparison between theory and experiment is aided by the use of a reliability factor

$$R_m=\Sigma(\chi_{\mathrm{th}}-\chi_{\mathrm{ex}})^2/\Sigma(\chi_{\mathrm{th}}^2+\chi_{\mathrm{ex}}^2), \tag{2}$$

where a value of 0 corresponds to perfect agreement, a value of 1 to uncorrelated data, and a value of 2 to anticorrelated data.[23,24] The search in parameter space to locate the structure having the minimum R-factor was helped by the use of a Marquardt algorithm, in which the calculation of the curvatures can be made considerably faster by using the so-called linear method.[27] In order to estimate the errors associated with the individual structural parameters we use an approach based on that of Pendry which was derived for LEED.[28] This involves defining a variance in the minimum of the R-factor, R_{min} as

$$\mathrm{Var}=R_{\mathrm{min}}\sqrt{(2/N)}, \tag{3}$$

where N is the number of independent pieces of structural information contained in the set of modulation functions used in the analysis. All parameter values giving structures with R-factors less than $R_{\mathrm{min}}+\mathrm{Var}(R_{\mathrm{min}})$ are regarded as falling within one standard deviation of the ''best fit'' structure. More details of this approach, in particular on the definition of N, can be found in a recent publication.[29]

III. EXPERIMENTAL DETAILS

The experiments were conducted at the BESSY synchrotron facility in Berlin on the HE-TGM-1 beamline.[30] The purpose-built UHV chamber is equipped with sample heating and cooling facilities, an Ar-ion sputter gun, LEED optics and a concentric spherical sector electron spectrometer (VG Scientific, 152 mm radius, three channeltron detector) for soft x-ray photoelectron spectroscopy to allow characterization of surface cleanness as well as to measure the photoelectron diffraction spectra. The Cu{110} crystal was initially prepared by x-ray Laue-orientation, spark-erosion and mechanical as well as electrochemical polishing, and was prepared in situ by Ar-ion bombardment and annealing (800 K) cycles until a well ordered surface with no detectable contamination was formed. The pyridine (99.9%) was admitted to the surface by backfilling the chamber with pyridine vapor. After forming a saturated layer by dosing 7

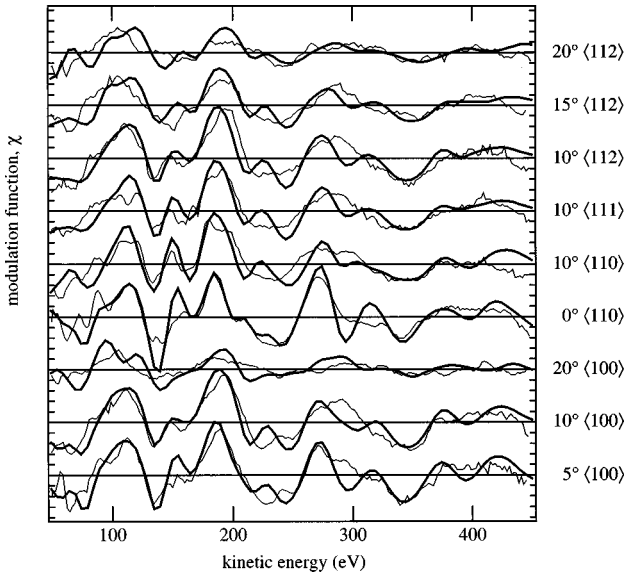

FIG. 2. Experimental PhD modulation functions (fine lines) used in the structure optimization together with the theoretically simulations (bold lines) for the optimum geometry shown in Fig. 6.

$\times 10^{-6}$ mbar s pyridine at 120 K sample temperature the crystal was slowly heated to 185 K. Comparing the C 1*s* core-level intensity of this pyridine layer with the C 1*s* intensity in the system Ni{110}$c(2\times4)-C_2H_4$ at $\theta=0.5$ we estimate that the pyridine coverage is approximately $\theta=0.4$, where one monolayer corresponds to one molecule per surface Cu atom.

Photoelectron diffraction spectra were only recorded for the N 1*s* core level, since the C 1*s* core level signal showed only marginal diffraction effects due to the presence of several inequivalent C atoms contributing incoherently to the diffraction pattern. The N 1*s* PhD spectra were measured in the kinetic energy range 50–450 eV in the four main azimuthal directions ⟨110⟩, ⟨111⟩, ⟨211⟩, and ⟨100⟩ for polar angles between 0° and 60° in steps of 10°. The signal was recorded at successive photon energies (separated by 2 eV) for kinetic energies of about ±25 eV around the N 1*s* core level peak to give a series of energy distribution curves (EDCs). The intensity of each of these peaks was then determined by background subtraction and integration, and the resulting intensity-energy spectra were normalized to give the modulation functions defined above. After integration and normalization, nine modulation functions were selected for the full quantitative structure optimization described in the next section. These modulation functions are shown as the fine curves in Fig. 2.

IV. STRUCTURE DETERMINATION

The experimental PhD modulation functions of Fig. 2 show strong intensity oscillations in near normal emission, but the modulation amplitude decays rapidly with increasing polar emission angle until at 20° off-normal emission they are barely distinguishable from the scatter in the data. This behavior is typical for atop, or near atop, adsorption where the normal emission spectrum is dominated by the backscattering event at the underlying Cu atom. The application

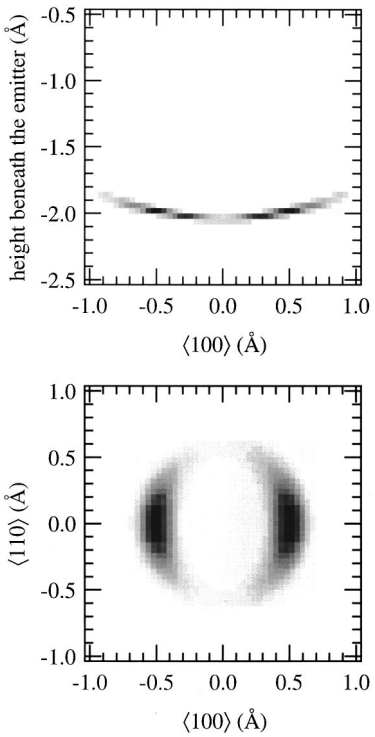

FIG. 3. Result of the application of the projection method to the full N 1*s* PhD data set. The emitter is located at (0, 0, 0). The top diagram shows the projection coefficient in a plane perpendicular to the surface through the emitter. The bottom diagram is a cut parallel to the surface at a height of 2 Å below the emitter.

of the projection method to the full data set (all polar angles in all four azimuths) supports this preliminary conclusion. Figure 3 shows the projection coefficient in a plane perpendicular to the surface through the emitter and in a plane parallel to the surface approximately 2 Å below the emitter. Both images are dominated by two areas corresponding to high values of the projection coefficents (dark regions in the gray-scale plot), indicating the presence of a neighboring Cu atom approximately 2 Å below the N-atom. The splitting in the ⟨100⟩ direction suggests that the N atom is not located exactly in an atop position but is displaced by about 0.5 Å in the ⟨100⟩ direction. The twofold rotational symmetry of the ''image'' reflects the existence of at least two energetically equivalent domains, as would be expected for a low symmetry adsorption site.

This near atop site served as a starting point for the structure optimization using full multiple scattering calculations. In these simulations the position of the N atom as well as the orientation of the molecular plane were optimized. It was first assumed that the N atom is bonded near atop a Cu atom in the first layer, i.e., above a Cu atom in the outermost close-packed rows in the ⟨110⟩ direction. In order to quantify how the ring orientation affects the simulated N 1*s* PhD modulation functions, the ring position in three dimensions, and thus the N-atom position, were optimized for a set of different ring orientations covering all possibilities within physically reasonable limits. The internal structural parameters have been fixed at the values corresponding to the free molecule. Molecular orientation is characterized by the Euler

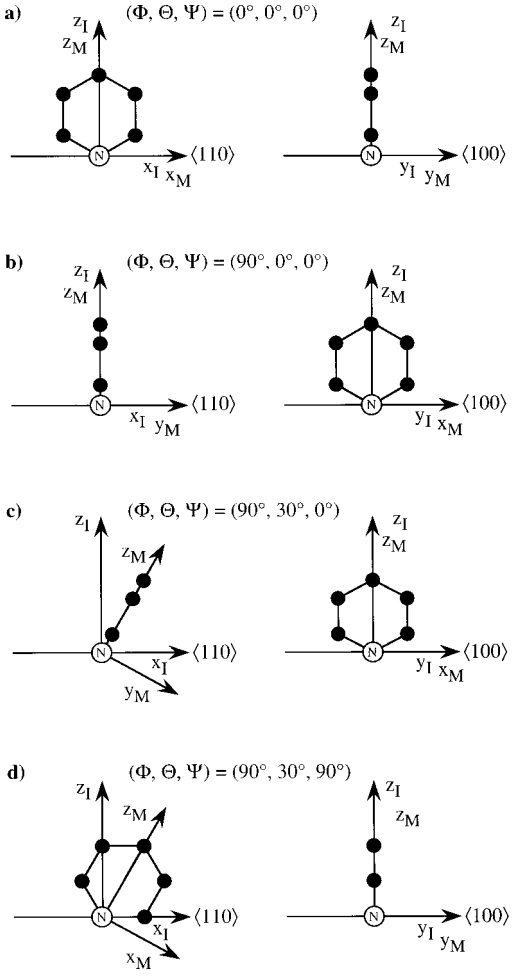

FIG. 4. Examples of some orientations of the aromatic ring together with the corresponding Euler angles (Φ, Θ, Ψ), which are used as parameters in the multiple scattering calculations. Each example (a)–(d) shows a front and a side view of the pyridine molecule and its orientation with respect to the surface. Also shown are the two coordinate systems (x_I, y_I, z_I) and (x_M, y_M, z_M) which are fixed relative to the surface and the molecule, respectively, and which are related by the Euler angles.

angles Φ, Θ, and Ψ, each of which corresponds to rotation of the ring plane about a particular axis. Figure 4 defines the axes involved and also shows some examples including the case of $\Phi = \Theta = \Psi = 0°$ [Fig. 4(a)] which corresponds to the upright molecule with the ring plane oriented in the ⟨110⟩ azimuth, i.e., parallel to the direction of the close-packed rows of the {110} surface. The Euler angles relate the coordinate systems (x_I, y_I, z_I) and (x_M, y_M, z_M) which are fixed relative to the crystal surface and the molecule, respectively. Note that the order of application of the three angular rotations is also uniquely defined in this convention.

Figure 5 shows the best *R*-factors obtained for different ring orientations by optimizing the ring position (and thus the N atom position) for each orientation. The left-hand side of the diagram ($\Psi = 0°$) shows the *R*-factors as a function of Θ (which, according to the definitions above, corresponds to a tilt of the C_2 axis of the free molecule with respect to the surface normal) for three different azimuthal orientations of the ring plane ($\Phi = 0°$, 45°, and 90°). The right-hand side ($\Psi = 90°$) shows *R*-factors for $\Phi = 0°$, 45°, and 90° as a function of Θ; the molecular plane remains perpendicular to

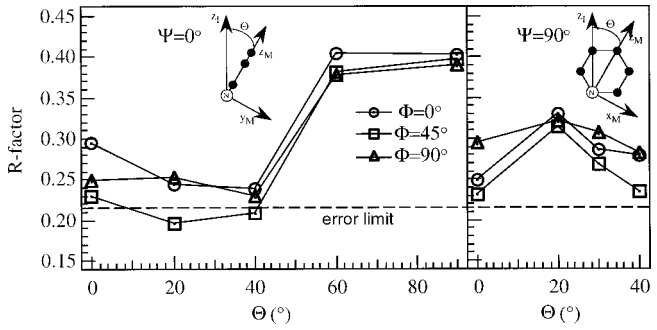

FIG. 5. *R*-factors for different ring orientations. The ring position, and thus the N atom position, has been optimized for each point, whereas the internal molecular geometry has been assumed to be the same as in the free molecule.

the surface in this case. First, the diagram shows clearly that the *R*-factor is sensitive to the orientation of the molecular plane, even though the C atoms are relatively weak scatterers. Secondly, all *R*-factors for $\Psi = 90°$ are outside the error limit, defined by the minimum *R*-factor (0.190) plus the variance of 0.024 and indicated by the horizontal line in Fig. 5. This finding allows us to exclude immediately the formation of an α-pyridyl species which would correspond to the $\Psi = 90°$ geometries on the right-hand side of Fig. 5. The best *R*-factor of 0.190 was obtained for $(\Phi, \Theta, \Psi) = (45°, 20°, 0°)$ which corresponds to a molecule with the molecular plane twisted azimuthally by 45° with respect to the ⟨110⟩ direction and tilted by 20° relative to the surface normal. All other ring orientations gave *R*-factors outside the variance. The optimization of the ring position at this orientation places the N atom in a site 0.25 Å away from the atop site in approximately ⟨112⟩ direction, which corresponds to a tilt of the N–Cu bond of approximately 8° relative to the surface normal. From the orientation of the ring together with the N atom position one can conclude that the ring plane as well as the N–Cu axis are tilted away from the atop site and that the ring plane is oriented perpendicular to that tilt direction. So far only a near-atop site above a Cu atom in the close-packed rows has been considered. A final step in this stage of the analysis was to consider the possibility of adsorption atop a second layer Cu atom in the troughs, as this could also be consistent with the results of the projection method. This model gave, however, a best *R*-factor of only 0.25 which is outside the variance.

For the structural optimisations shown in Fig. 5 the parameters Φ, Θ, and Ψ describing the ring orientation were assigned discrete values. In the last stage of the structure determination the best geometry which is near $(\Phi, \Theta, \Psi) = (45°, 20°, 0°)$ was optimized by varying all parameters continuously and in parallel. These were the three angles Φ, Θ, and Ψ, the N atom position (and thus the ring position in three dimensions) as well as the isotropic vibrational amplitude of the N atom. The corresponding best fit parameter values are listed in Table I; the *R*-factor improved only marginally from 0.190 to 0.185. Figure 6 shows the optimized adsorption geometry and the calculated modulation functions for this structure are shown in Fig. 2 as bold curves. The final results show that the N atom adsorbs near-atop a Cu

TABLE I. Parameters obtained for the best fit between the experimental data and theoretical simulations. The estimated errors are also shown.

Parameter	Optimized value
d_{N-Cu}	2.00 ($\pm$0.02) Å
ξ_{N-Cu}	8 ($\pm$5)°
λ_{N-Cu}	120 ($\pm$90)°
Φ	60 (+15, −28)°
Θ	20 ($\pm$15)°
Ψ	0 ($\pm$15)°
$\langle u^2 \rangle$	$6.5(+2.4/-2.0)\times10^{-3}$ Å^2

atom in the close-packed rows with a N–Cu bond length d_{N-Cu} of 2.00 ($\pm$0.02) Å. The N–Cu bond axis is tilted by $\zeta_{N-Cu}=8(\pm5)°$ relative to the surface normal in approximately the $\langle 112 \rangle$ direction. This corresponds to $\lambda_{N-Cu}=120(\pm90)°$, where the error bar also includes all other high symmetry directions (see below). The molecular plane is rotated by $\Phi=60(+15/-28)°$ relative to the $\langle 110 \rangle$ direction and tilted by $\Theta=20(\pm15)°$ away from the surface normal. We note that tilt angles of 8° for the Cu–N axis and 20° for the ''C_2'' axis might imply that they are not coplanar and that some degree of rehybridization has taken place at the N atom. However, the coplanar values are just inside the respective error bars. For the isotropic vibrational amplitude of the N atom $\langle u^2 \rangle$ we obtained a value of $6.5(+2.4/-2.0)\times10^{-3}$ Å^2.

The error bars for all parameters were determined by varying the parameter in question in discrete steps and subsequently optimizing all other parameters for each step. The error limit for the parameter is then the value where the optimisation gives an *R*-factor of 0.208 corresponding to the minimum *R*-factor (0.185) plus the variance (0.023). This strategy for determining the error bars gives values that are upper limits and includes any possible effects of parameter coupling. In the present system a coupling of the chosen parameters is quite likely to occur but is difficult to predict in advance. The usual method of determining the error bars from the curvature of the *R*-factor surface at the minimum could significantly underestimate the errors associated with the coupled parameters.

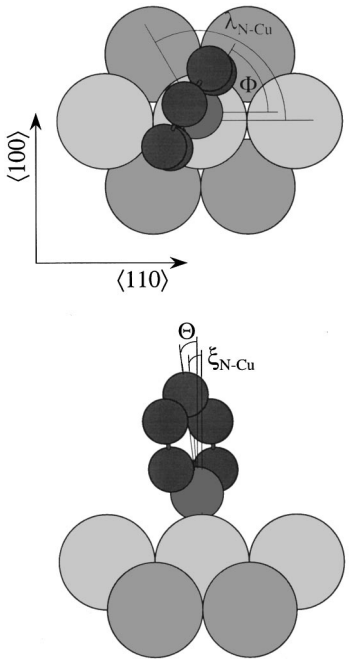

FIG. 6. Optimized local adsorption geometry of pyridine on Cu{110}.

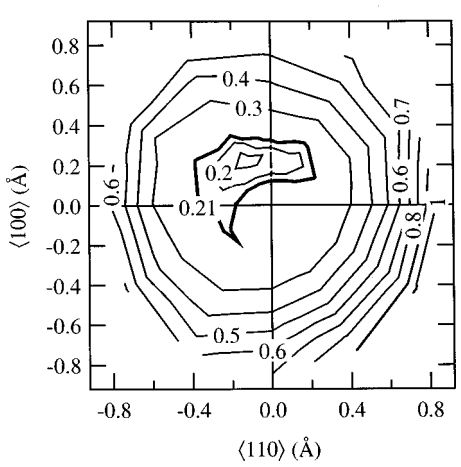

FIG. 7. Contour diagram showing the *R*-factor as a function of the lateral shift of the N atom away from the atop site. The N–Cu bond length and the ring orientation have been fixed at their optimum values. The bold line gives the error limit.

V. DISCUSSION

A. Photoelectron diffraction aspects

From the point of view of the experimental technique the major result reported in the present paper is the astonishingly high sensitivity of the *R*-factor to the orientation of the aromatic ring. We have therefore looked at this issue in more detail. Figure 7 shows a contour plot of the *R*-factor as a function of the position of the N atom parallel to the surface in the region around the exact atop position. The N–Cu bond length has been set at the optimum value of 2.00 Å and the ring orientation has also been fixed at its best fit value. The bold contour line corresponds to the upper limit of acceptable *R*-factor values, so all structures falling within this contour are within our error limits. The first observation is that the *R*-factor is very insensitive to the lateral position of the N atom. This is well known from our previous work on atop adsorption systems, e.g., the C atoms in C_2H_4 on Ni{111},[31] and is due to the low sensitivity of the high amplitude, normal emission modulation function to small changes in the scattering angle. A second, more subtle feature of the contour plot is the absence of 2mm rotational and mirror symmetry of the substrate. In discussing this aspect of Fig. 7 it is important to distinguish between the mode of data presentation used in this contour plot and the way the PhD calculations are performed. In any adsorption structure which has a symmetry lower than that of the substrate point group, the role of equal occupation of other sites related by the missing operations of the point group must be included. This ''domain averaging'' is therefore always included in the simulations. The structures represented in Fig. 7 include a molecular orientation which is fixed as the molecule is moved

across the surface, so the upper left-hand quarter of the map corresponds to geometries in which the molecular ring is tilted away from the atop site (in the same direction as the N atom offset from atop) while in the lower right-hand quarter the tilt is towards atop (in the opposite sense to the N-atom offset). The reduced symmetry of Fig. 7 is therefore direct evidence that both substrate scattering and intramolecular scattering are important in determining the fit of the theoretical and experimental PhD spectra. If only substrate scattering were important then the plot would retain the 2mm symmetry of the equivalent N sites. If only intramolecular scattering were to be important, the *R*-factor would not vary across the contour map.

Ideally, C 1*s* photoelectron diffraction data should be used for determining the co-ordinates of the C atoms of the ring, but these occur in at least three different environments in this molecule. Their corresponding C 1*s* lines are not resolvable using our present instrumentation and, hence, a PhD analysis of the individual spectral components—which we have termed elsewhere[32,33] ''chemical shift'' photoelectron diffraction—is not possible at the moment. This problem can be overcome in future by utilizing third generation synchrotron radiation sources which will provide higher spectral resolution at equivalent, or even higher, sensitivity.

A second point to address is the coupling in the analysis of the parameters defining the amplitude of the vibrations of the emitter to the lateral shift away from the exact atop position. As mentioned above, the isotropic vibrational amplitude of the N atom was optimized in parallel with all other parameters. On the other hand, if the N atom is fixed exactly atop but allowed to vibrate anisotropically, the lateral vibrational amplitude turns out to be much larger than the perpendicular one. The optimum *R*-factor for this situation is 0.20 and lies within the variance of the geometry shown in Fig. 6. This coupling of the dynamic and static shifts away from high symmetry sites has been observed for other systems involving atop sites, such as NH_3 on Cu{110},[29] and also for an imide species (NH) which occupies a bridge site on the same surface.[34] It may be possible to draw a clear distinction between the two cases, i.e., between a low symmetry adsorption site and the strict atop geometry with high lateral vibrational amplitudes, by performing temperature-dependent measurements down to cryogenic temperatures where dynamic effects are eliminated. Studies at lower coverage—a point we return to below—would also be interesting in this context, particularly if an atop adsorption site with strongly anisotropic emitter vibrations were to be found for this putatively higher symmetry geometry (C_{2v}) (Ref. 16).

B. Pyridine surface chemistry

As we have remarked in the Introduction, the adsorption behavior of pyridine depends on both coverage and temperature as well as on the particular metal surface. Thus, at low coverage and low temperature, adsorption on Ag{111},[6,7] Ni{100},[8] Ni{111},[9–11] Ru{001},[12,13] and Pd{110} (Ref. 14) gives rise to a parallel, or nearly parallel, species. On Ir{111} (Ref. 17) the ring plane was found with ESDIAD to be nearly perpendicular to the surface (angle of inclination $\approx 20°$ in three equivalent azimuths), but there appears to be no data for low coverage. The behavior on Pt{111} (Refs. 12, 16, 18, 19) is complicated in that there is evidence for a substantial angle of inclination of the molecular plane or, alternatively, for a mixture of parallel and perpendicular species. Moreover, at room temperature on Pt{111} the C–H bond adjacent to the N atom breaks and a bidentate α-pyridyl species (C_5H_4N) is formed.[12,16,18,19] The latter could bond either perpendicular to the surface, as shown in Fig. 1(d) or with the molecular plane inclined [Fig. 1(e)] if the π-system is sufficiently strongly involved in bonding. The α-pyridyl species has also been observed on Ru{001} (Refs. 12, 13) and Ni{100}.[8] Changes in orientation from parallel to upright as a function of increasing coverage, which has aptly been referred to as a crowding effect,[12] are well documented for pyridine on Ag{111} (Refs. 6, 7) and Ni{100}.[8] Thus, Bader *et al.*[7] showed in their NEXAFS study on Ag{111} that the mean angle of inclination relative to the surface normal changes from about 45° to 70° as a function of increasing coverage. Although the accuracy of such angle determinations in NEXAFS is not particularly great, these and other, similar data have demonstrated dramatically the presence of such effects. Vibrational spectroscopy, photoemission, and NEXAFS indicate, however, that for pyridine on Cu{110} the ring plane is *perpendicular to the surface at low coverage*.[12,15,16] (The NEXAFS study of Bader *et al.*[15] was presumably carried out on a layer of relatively low coverage; an exposure of 1 langmuir is given.) The ring plane was found to be oriented perpendicular to the surface within $\pm 10°$; interestingly, it was also found to be strongly aligned in the ⟨100⟩ azimuth, i.e., perpendicular to the close-packed rows. As expected, the perpendicular geometry still pertains at higher coverage, although the appearance of an additional band in the vibrational spectrum has been interpreted in terms of symmetry lowering due to a ''tilting back'' toward the surface plane.[16]

The present results indicate that on Cu{110} the extent of the tilt ($\approx 20°$) is still relatively small at high coverage and comparable to that measured for pyridine on Ir{111} with ESDIAD (Ref. 17) and (considering the estimated precision) significantly smaller than that measured on Ag{111} with NEXAFS.[7] Haq and King[16] interpret the appearance of a ring mode at 1436 cm^{-1} (which belongs to B_2 under C_{2v}) in terms of the C_2 axis of the (free) molecule being no longer perpendicular to the surface plane. We confirm that the C_2 axis is indeed not perpendicular to the surface at high coverage. Unfortunately, due to lack of sensitivity (something which will also be remedied by third generation sources), we were unable to perform measurements at lower coverages. The possibility remains, however, that the angle of inclination at low surface concentration is the same, but that the symmetry lowering is actually due to the adoption of the off-atop site. The strong adsorbate–adsorbate interaction is consistent with the fact that the distance between neighboring molecules must be of the order of 5 Å and thus similar to the nearest neighbor separation in the molecular crystal.[35]

Finally, we note that the perpendicular geometry of pyridine on Cu{110} over the whole range from zero coverage to a saturated layer is probably due to the fact that bonding via the N lone pair is more important than the interaction

with the π electrons of the aromatic ring. The interaction is weak with considerable desorption having occurred by 250 K (Ref. 16) and there is no report of α-pyridyl formation. This is similar to the situation encountered in CO adsorption on copper surfaces; adsorption is weak and 5σ donation is considered to provide a less important contribution to the bond than $d-\pi^*$ backdonation.[36] (A synergic bonding mechanism, similar to that in the corresponding organometallic complexes, is thought to occur for benzene and other aromatics on metal surfaces.[2,3]) This analogy does not work for silver, however, where CO appears only to physisorb;[37] on this surface pyridine adopts a near-parallel configuration at low coverages.

VI. SUMMARY

The adsorption site as well as the ring orientation of pyridine on Cu(110) have been determined with scanned-energy mode photoelectron diffraction. At a coverage of approximately $\theta=0.4$ the molecule adsorbs near atop a Cu atom in the close-packed Cu rows with a N–Cu bond length of 2.00 ($\pm$0.02) Å. The N atom is tilted away from the atop site by 8 ($\pm$5)° in approximately the $\langle 112\rangle$ direction. The molecular plane is turned by 60 ($+15/-28$)° away from the $\langle 110\rangle$ direction and the molecule is tilted by 20 ($\pm$15)° with respect to the surface normal. The adsorption geometry confirms that the pyridine molecule stays intact upon adsorption and does not form an α-pyridyl species. The ring orientation could be determined with surprisingly high precision, even though only N 1*s* PhD modulation functions have been used for the structure determination. Multiple scattering events involving a substrate Cu atom and a C atom in the ring, and not forward scattering, provide the sensitivity to ring orientation. The existence of a molecular tilt, albeit a relatively small one, at these high coverages confirms the result of a recent study with vibrational spectroscopy. It is not clear, however, whether the observed symmetry lowering in that experiment results from this effect.

ACKNOWLEDGMENTS

This work has been supported by the German Federal Ministry of Education, Science, Research and Technology (Contract No. 05 625EBA 6), by the Engineering and Physical Science Research Council (UK) and by the European Union through a HCM Network (Grant No. ERBFMGF CT 950031) and through the Large Facilities program. The authors thank Volker Fritzsche for providing the multiple scattering codes. A.M.B. and D.P.W. are grateful to the Humboldt Foundation and the Max-Planck Society for additional support.

[1] N. Sheppard and C. de la Cruz, Adv. Catal. **42**, 181 (1998).
[2] F. P. Netzer and M. G. Ramsey, Crit. Rev. Solid State Mater. Sci. **17**, 397 (1992).
[3] A. M. Bradshaw, Surf. Sci. **331-333**, 978 (1995); Curr. Opin. Solid State Mater. Sci. **2**, 530 (1997).
[4] C. Stellwag, G. Held, and D. Menzel, Surf. Sci. **325**, L379 (1995), and references therein.
[5] O. Schaff, V. Fernandez, Ph. Hofmann, K-M. Schindler, A. Theobald, V. Fritzsche, A. M. Bradshaw, R. Davis, and D. P. Woodruff, Surf. Sci. **348**, 89 (1996); G. Held, Mp. P. Bessent, S. Titmuss, and D. A. King, J. Chem. Phys. **105**, 11305 (1996).
[6] J. E. Demuth, K. Christmann, and P. N. Sanda, Chem. Phys. Lett. **76**, 201 (1980).
[7] M. Bader, J. Haase, K.-H. Frank, A. Puschmann, and A. Otto, Phys. Rev. Lett. **56**, 1921 (1986).
[8] N. J. DiNardo, Ph. Avouris, and J. E. Demuth, J. Chem. Phys. **81**, 2169 (1984).
[9] M. R. Cohen and R. P. Merrill, Langmuir **6**, 1282 (1990).
[10] S. Aminpirooz, L. Becker, B. Hillert, and J. Haase, Surf. Sci. Lett. **244**, L152 (1991).
[11] V. Fritzsche, S. Bao, Ph. Hofmann, M. Polcik, K.-M. Schindler, and A. M. Bradshaw, Surf. Sci. **319**, L1 (1994).
[12] M. E. Bridge, M. Connolly, D. R. Lloyd, J. Somers, P. Jakob, and D. Menzel, Spectrochim. Acta A **43**, 1473 (1987).
[13] P. Jakob, D. R. Lloyd, and D. Menzel, Surf. Sci. **227**, 325 (1990).
[14] F. P. Netzer, G. Rangelov, G. Rosina, and H. B. Saalfeld, J. Chem. Phys. **89**, 3331 (1988).
[15] M. Bader, J. Haase, K.-H. Frank, C. Ocal, and A. Puschmann, J. Phys. Colloq. **47**, C8-491 (1986).
[16] S. Haq and D. A. King, J. Phys. Chem. **100**, 16957 (1996).
[17] J. U. Mack, E. Bertel, and F. P. Netzer, Surf. Sci. **159**, 265 (1985).
[18] A. L. Johnson, E. L. Muetterties, J. Stöhr, and F. Sette, J. Phys. Chem. **89**, 4071 (1985).
[19] V. H. Grassian and E. L. Muetterties, J. Phys. Chem. **90**, 5900 (1986).
[20] F. P. Netzer and E. Rangelov, Surf. Sci. **225**, 260 (1990).
[21] A. Bruckbauer and A. Otto, J. Raman Spectrosc. **29**, 665 (1998).
[22] D. P. Woodruff and A. M. Bradshaw, Rep. Prog. Phys. **57**, 1029 (1994).
[23] Ph. Hofmann, K.-M. Schindler, S. Bao, V. Fritzsche, A. M. Bradshaw, and D. P. Woodruff, Surf. Sci. **337**, 169 (1995).
[24] Ph. Hofmann and K.-M. Schindler, Phys. Rev. B **47**, 13941 (1993); Ph. Hofmann, K.-M. Schindler, S. Bao, A. M. Bradshaw, and D. P. Woodruff, Nature (London) **368**, 131 (1994).
[25] V. Fritzsche, J. Phys.: Condens. Matter **2**, 1413 (1990); Surf. Sci. **265**, 187 (1992).
[26] V. Fritzsche, Surf. Sci. **213**, 648 (1986).
[27] V. Fritzsche and J. B. Pendry, Phys. Rev. B **48**, 9054 (1993).
[28] J. B. Pendry, J. Phys. C **13**, 937 (1980).
[29] N. A. Booth, R. Davis, R. Toomes, D. P. Woodruff, C. Hirschmugl, K.-M. Schindler, O. Schaff, V. Fernandez, A. Theobald, Ph. Hofmann, R. Lindsay, T. Gießel, P. Baumgärtel, and A. M. Bradshaw, Surf. Sci. **387**, 152 (1997).
[30] E. Dietz, W. Braun, A. M. Bradshaw, and R. L. Johnson, Nucl. Instrum. Methods **239**, 359 (1985).
[31] S. Bao, Ph. Hofmann, K.-M. Schindler, V. Fritzsche, A. M. Bradshaw, D. P. Woodruff, C. Casado, and M. C. Asensio, Surf. Sci. **323**, 19 (1995).
[32] K.-U. Weiss, R. Dippel, K.-M. Schindler, P. Gardner, V. Fritzsche, A. M. Bradshaw, A. L. D. Kilcoyne, and D. P. Woodruff, Phys. Rev. Lett. **69**, 3196 (1992).
[33] K.-U. Weiss, R. Dippel, K.-M. Schindler, P. Gardner, V. Fritzsche, A. M. Bradshaw, D. P. Woodruff, M. C. Asensio, and A. R. Gonzalez-Elipe, Phys. Rev. Lett. **71**, 581 (1992).
[34] C. J. Hirschmugl, K.-M. Schindler, O. Schaff, V. Fernandez, A. Theobald, P. Hofmann, A. M. Bradshaw, R. Davis, N. A. Booth, D. P. Woodruff, and V. Fritzsche, Surf. Sci. **352**, 232 (1996).
[35] D. Mootz and H.-G. Wussow, J. Chem. Phys. **75**, 1517 (1981).
[36] K. Hermann, P. S. Bagus, and C. J. Nelin, Phys. Rev. B **35**, 9467 (1987).
[37] S. Krause, C. Mariani, K. C. Prince, and K. Horn, Surf. Sci. **138**, 305 (1984).